Primary Mirror Segmentation Studies for the Thirty Meter Telescope†

Curtis Baffes*[a], Terry Mast[b], Jerry Nelson[b], Eric Ponslet[c], Vince Stephens[d], Larry Stepp[e], Eric C. Williams[e]
[a]Jet Propulsion Laboratory, California Institute of Technology, 4800 Oak Grove Drive, Pasadena, CA 91109, USA
[b]Center for Adaptive Optics, University of California, Santa Cruz, CA 95064, USA
[c]Formerly HYTEC, Inc.
[d]HYTEC Inc., 110 Eastgate Drive, Los Alamos, NM 87544, USA
[e]TMT Observatory Corp., 2632 E. Washington Blvd, Pasadena, CA 91107, USA

ABSTRACT

The Thirty Meter Telescope (TMT) project, a partnership between ACURA, Caltech, and the University of California, is currently developing a 30-meter diameter optical telescope. The primary mirror will be composed of 492 low expansion glass segments. Each segment is hexagonal, nominally measuring 1.44m across the corners. Because the TMT primary mirror is curved (i.e. not flat) and segmented with uniform 2.5mm nominal gaps, the resulting hexagonal segment outlines cannot all be identical. All segmentation approaches studied result in some combination of shape and size variations. These variations range from fractions of a millimeter to several millimeters. Segmentation schemes for the TMT primary mirror are described in some detail. Various segmentation approaches are considered, with the goal being to minimize various measures of shape variation between segments, thereby reducing overall design complexity and cost. Two radial scaling formulations are evaluated for their effectiveness at achieving these goals. Optimal tuning of these formulations and detailed statistics of the resulting segment shapes are provided. Finally, we present the rationale used for selecting the preferred segmentation approach for TMT.

Keywords: mirror, segment, segmentation, deformation, optics, correction, scaling, projection, irregularity

1. INTRODUCTION

1.1 Background

The Thirty Meter Telescope (TMT) Project[1], a partnership between ACURA, Caltech, and the University of California, is developing an astronomical observatory that will incorporate one of the first of the new generation of Extremely Large Telescopes (ELTs). The telescope utilizes a Ritchey-Chrétien optical design, with a 30m diameter primary mirror (M1) composed of 492 hexagonal segments. Each segment is made from low-expansion glass or glass ceramic, measures approximately 1.44m between opposite corners, and is separated from adjacent segments by 2.5mm wide gaps. The tip, tilt, and piston of each segment will be actively adjusted by three position actuators and monitored by an array of edge sensors (12 per segment). The edge sensors and position actuators work together to control relative segment positions such that the segments function as a continuous optical surface.

Inter-segment gaps are necessary to prevent contact between adjacent segments. Effects that can reduce the gaps and bring segments closer to each other include manufacturing and assembly tolerances, gravity and temperature-induced mirror cell deformations, and the coupling of tip/tilt actuation in to segment lateral motion. Given that the inter-segment gaps are required, it is optically desirable to keep the inter-segment gaps as small and as uniform as possible.

On a flat surface, it is possible to create an array of identical regular (i.e. equilateral and equiangular) hexagons separated by uniform gaps. However, on the aspheric curved surface of the primary mirror, it is not possible to create an array of

* cbaffes@tmt.org; phone 1 626 395-1632; fax 1 626 395-8909
† SPIE 7018-29, TMT.OPT.JOU.08.003.REL01, JPL CL#08-1541

hexagons that are regular *and* of equal size *and* separated by uniform gaps. This paper describes an approach to segmentation – defining the irregular hexagonal outlines of the segments such that uniform inter-segment gaps are maintained and various metrics describing their geometric shape are optimized.

1.2 Coordinate systems

The TMT Primary Mirror Coordinate System has two variants: one Cartesian and one cylindrical. For both the Cartesian and cylindrical systems, the origin is at the vertex of the primary mirror, and the Z_{M1} axis is normal to the theoretical optical surface at the vertex. For the Cartesian system, the X_{M1} axis is perpendicular to the Z_{M1} axis, and parallel to the telescope elevation axis. The Y_{M1} axis is orthogonal to X_{M1} and Z_{M1} such that X_{M1}, Y_{M1}, and Z_{M1} form a right handed system. The Y_{M1} axis points to the zenith when the telescope is looking to the horizon. For the cylindrical system, R_{M1} is the radial direction (in the XY_{M1} plane), and θ_{M1} is measured counterclockwise-positive from X_{M1}. These coordinate systems are shown schematically in Figure 1.

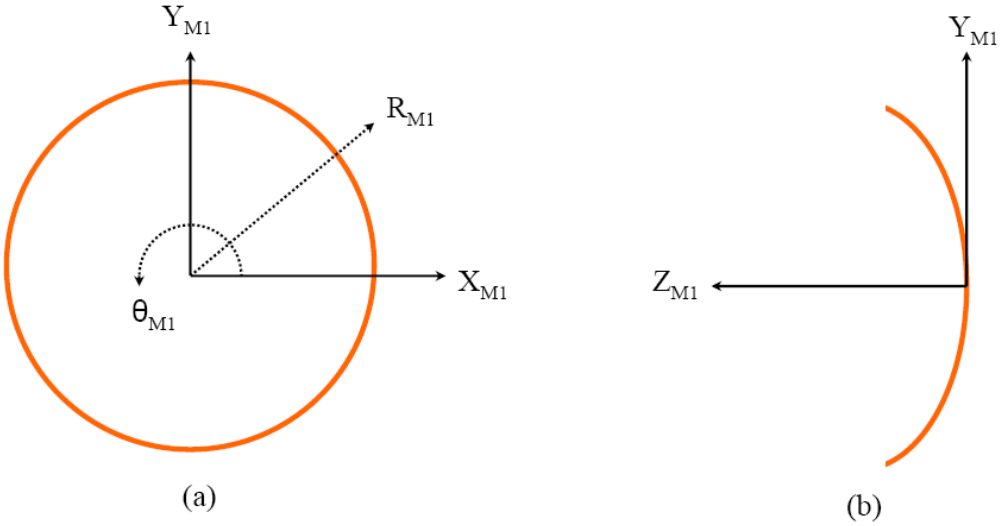

Fig. 1 TMT Primary Mirror Coordinate System. View (a) schematically represents the primary mirror, as seen from the stars. View (b) is a third-angle-projection from view (a).

1.3 Primary mirror architecture

The TMT primary mirror is a hyperboloid, with a paraxial radius of curvature k=60m and a conic constant of -1.000953. The array of 492 segments has six-fold symmetry; there are six identical sectors (A through F). Each sector contains 82 segments, each of which has a unique optical figure and hexagonal shape. A segment of a given type (e.g. Type 79) may be mounted in its assigned location within any of the six sectors of the primary mirror array. The definition of sectors and segment types is illustrated in Figure 2.

Each segment within the primary mirror is mounted on a Segment Support Assembly (SSA), as shown in Figure 3. The SSA[2,3] provides axial support (i.e. support parallel to the optical surface normal of the given segment) via a 27 point whiffletree mount. The SSA also supports the segment laterally using a central diaphragm flexure bonded in a pocket on the segment back surface.

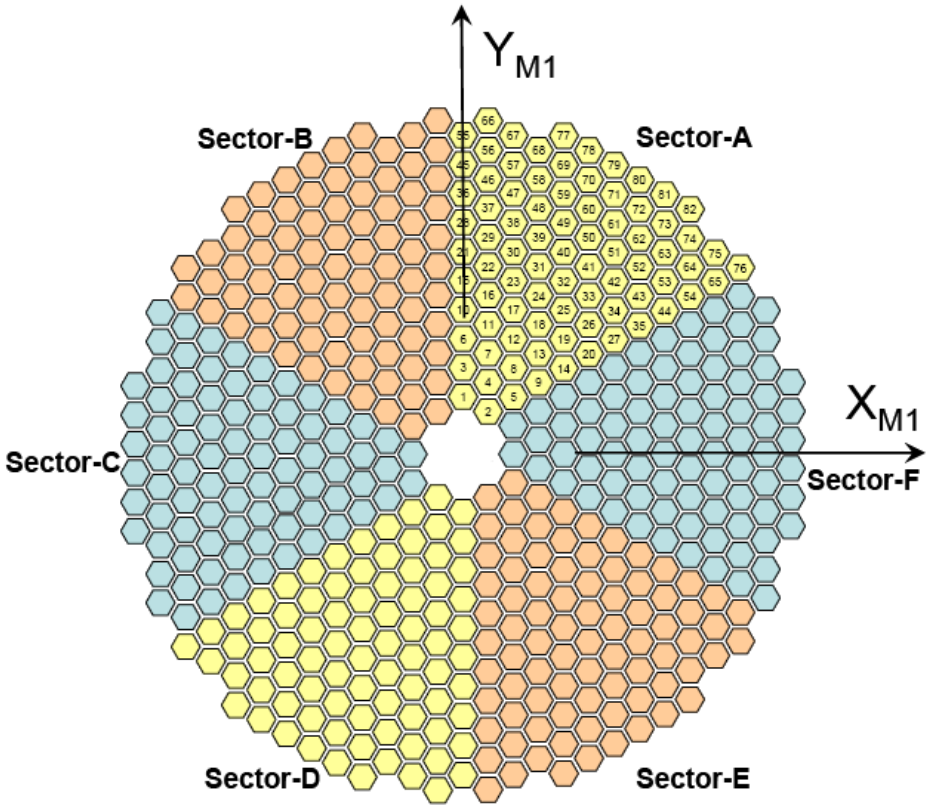

Fig. 2 Primary mirror sector and segment numbering scheme.

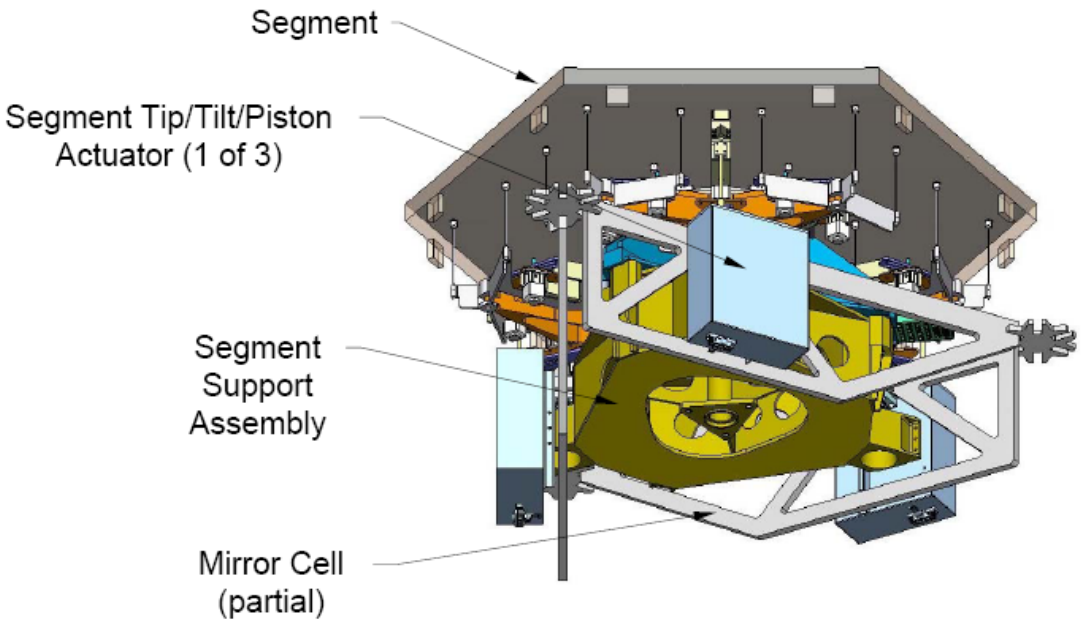

Fig. 3 A single segment, its Segment Support Assembly, actuators, and the portion of the Mirror Cell to which it is mounted.

All 492 SSAs are mounted to the Primary Mirror Cell, a large steel structure. The top layer of the Mirror Cell is a triangular lattice of planar trusses. The nodes of this lattice are aligned with segment vertices. Due to the six-fold symmetry of the array, the clocking of a given segment type increments by 60° between a given sector and an adjacent sector. To allow identical segment types to be interchanged, the SSAs must therefore clock as well. In order to facilitate this required clocking without complicating the geometry of the Mirror Cell, the interfaces between the SSAs and the Mirror Cell are located 1/3 of the way between the nodes of the Mirror Cell truss. This is illustrated in Figure 4. In this configuration, when the SSA is clocked by 60° degrees, the interface features are still located at a 1/3 point on a truss member, albeit with a different handedness. The interface features of sectors A, C, and E are considered right-handed, the interface features of sectors B, D, and F are, therefore, left-handed. Since the nodes and SSA-attachment locations of the Mirror Cell are defined with respect to the segments, the geometry of the Mirror Cell is also affected by the segmentation approach.

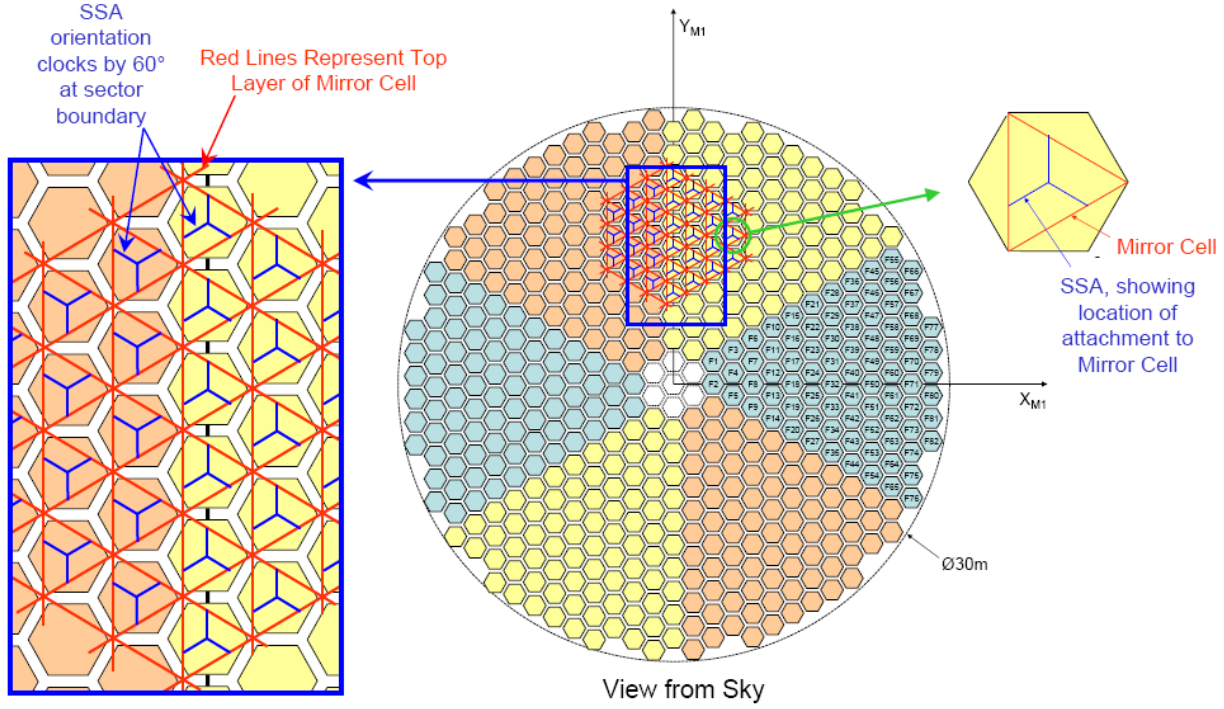

Fig. 4 Configuration of the Mirror Cell and attachment locations for the Segment Support Assemblies.

1.4 Segmentation approach used on the Keck telescopes

The W.M. Keck Observatory incorporates two segmented-mirror telescopes, each with a 10m diameter primary mirror. The segmentation approach used for the Keck telescopes, as described by Mast and Nelson[4], was as follows:

1. Define an array of regular, equally-sized hexagons in the XY_{M1} plane.
2. Project the hexagon corner locations along Z_{M1} to the optical surface.

Due to the curvature of the primary mirror, with increasing radial position, segments are elongated in the radial direction. This elongation is described by Mast and Nelson[4], and governed by the following equation:

$$E(R) = \frac{1}{\cos[\Phi(R)]} \tag{1}$$

Where *E(R)* is an elongation scale factor for the segment in the radial direction (relative to the hexagon in the base pattern in the XY plane), and $\Phi(R)$ is the angle of the surface at radius *R*, as shown in Figure 5.

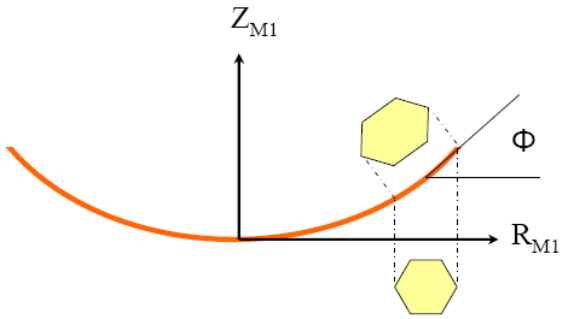

Fig. 5 Elongation of the segment shape caused by the segmentation scheme used for the Keck Telescope primary mirrors.

For the 1.8m Keck primary mirror segments, the largest elongation scale factor was 1.010, resulting in an 18mm elongation (corner to corner) of the outermost segments[4]. Were the Keck segmentation approach used for the 1.4m TMT primary mirror segments, the elongation of the outermost segment (corner to corner) would be approximately 45mm. Segment size and shape variations lead to a few undesirable consequences. The performance of the whiffletree system (i.e. the surface figure of the supported mirror) is very sensitive to the mass distribution of the supported mirror segment. Variation in segment profile leads to variation in segment mass distribution, which must be compensated for by the SSA design. Another consequence of highly variable geometry is that the segment blank, the circular meniscus from which hexagonal segments are cut, must be large enough to accommodate the largest segment in the array. For the smaller segments, the blanks would be over-sized, resulting in expensive material being removed and discarded.

1.5 Compensation for segmentation effects

It was recognized by the designers of the W. M. Keck Observatory that the segment size and shape variations had to be accounted for in the design of the whiffletree support system, or they would have severe optical consequences in terms of axial-gravity distortion of the optical surface as the telescope changes zenith angle. The Keck design uses *super-hex weights* to compensate for these segment size and shape variations. The *super-hex weights* are a set of small, discrete lead pieces that are bonded to the back surface, near the perimeter of each segment. These weights serve to adjust the total mass and the mass distribution of each segment to be the equivalent of a *super-hexagon* whose regular-hexagonal outline envelopes all the actual segment outlines. Using this method, one common support system was designed and optimized for supporting the *super-hexagon*. This support system was utilized to support the actual segments (loaded with *super-hex* weights) to achieve the required optical performance.

The super-hex method is one approach to solving the problem of compensating for segment shape and size variations. As will be described later, this approach has not been chosen for TMT because of the inefficiency of adding weights to each segment in terms of part count, added mass, and complexity. Additionally, the use of adhesives, having high coefficients of thermal expansion, to attach the super-hex weights to the back surface of the mirrors would be a thermal distortion concern for the relatively thin TMT mirrors.

Another approach considered for TMT was to add the super-hex weights to the whiffletree components, rather than the mirror surface. This is also an effective approach from an optical performance standpoint, but retains the complication of having to add up to 24 masses to each SSA. As with the super-hex weights, the inefficiency of adding weights to each whiffletree in terms of part count, added mass, and complexity led us to seek another approach.

A third compensation approach was considered and adopted for TMT that does not add weights or increase part-count. The TMT approach re-balances the whiffletrees to minimize surface error by shifting the locations of the whiffletree pivots. A plan view of the whiffletree layout is shown in Figure 6. Three pivots are mounted to the moving frame assembly (a rigid structure that serves as “ground”). A large triangle is mounted to each of these pivots. Each large triangle supports three more pivots, to which small triangles are mounted. Each small triangle axially supports the segment via three rod flexures. In total, the whiffletree incorporates 27 mirror support points and 12 pivots. By shifting the locations of the 12 pivots in two degrees of freedom each, up to 24 bending moments are introduced into the whiffletrees. These moments act upon the mirror to cancel the effects of imbalance due to irregular segment shape. The

basic premise is shown schematically in Figure 7. By translating the pivots that connect the various layers of the whiffletree (without moving the whiffletree triangles), it is possible to adjust the load distribution in the rod flexures supporting the segment and compensate for segment shape variations. This method has a low part count, however, the approach requires the production of 82 unique whiffletree sets, each having a specific set of pivot hole locations. All of the whiffletree parts are identical, except for the location of the twelve sets of pivot holes. In production, each segment type will be supported by its matching SSA type.

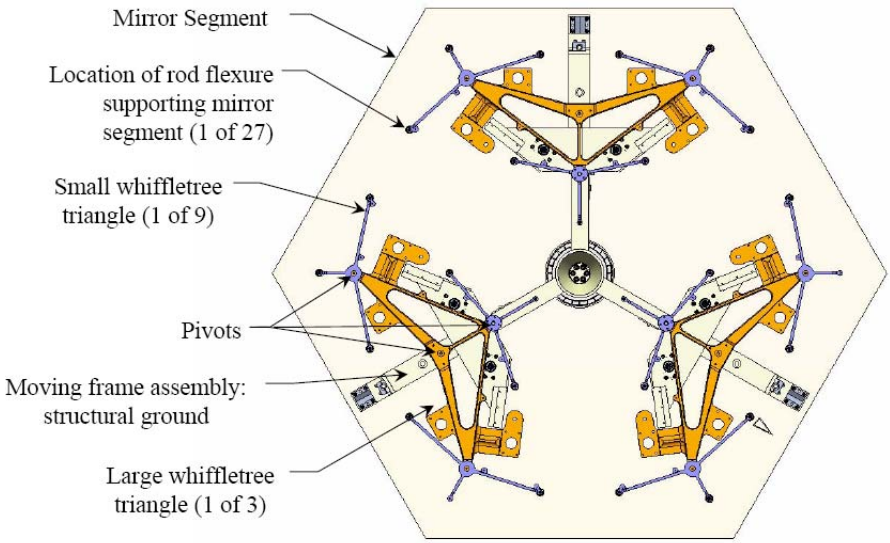

Fig. 6. Plan view of the key components of the axial support whiffletree. Shown are the moving frame assembly (which serves as structural "ground" for the axial support system), the whiffletree triangles and pivots, and the segment. For clarity, numerous components are not shown.

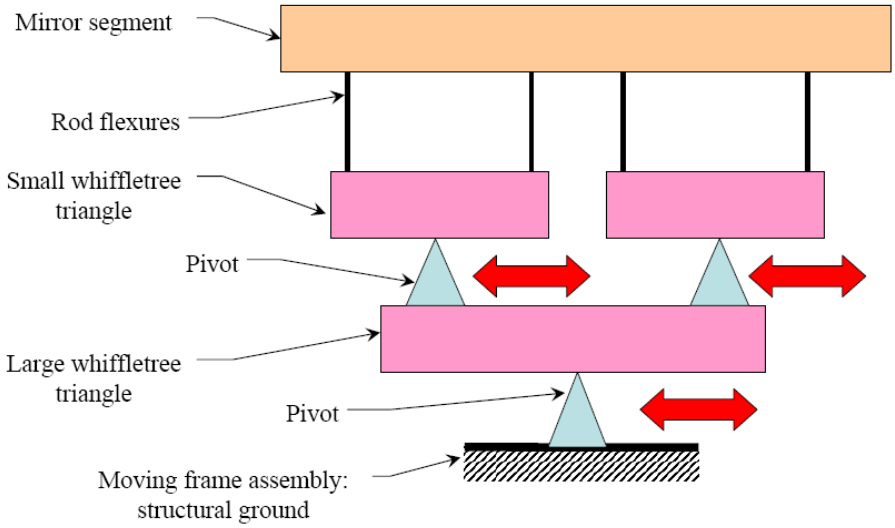

Fig. 7. Two-dimensional schematic representation of a single whiffletree showing the pivot-shift method of compensating for segment shape variation. Note that this is a two-dimensional representation of a three-dimensional system. In the three-dimensional system, each large whiffletree triangle supports three small whiffletree triangles, each of which accommodates three rod flexures. Each pivot can shift in two degrees of freedom.

It should be noted that none of the three compensation methods listed above is able to perfectly compensate for the segment size and shape variations. In the presence of an axial gravity load, an irregular, compensated segment will exhibit a residual surface error (relative to a regular, nominal segment under the same loading). For the pivot shifting method chosen for TMT, a sensitivity analysis was performed to determine the effect of segment size variations and seven postulated types of segment shape variations. This analysis calculated the required magnitude of pivot shifts, and the residual surface error after correction. These residual errors add in quadrature to the gravity-induced surface error of a nominal, regular segment. The results of the analyses of specific cases were used to develop formulas to estimate pivot shifts and residual surface error for generalized cases. The formulas are presented in 2.2.7 and 2.2.8.

2. METHODOLOGY

2.1 Segmentation approach

In order to minimize the effects caused by segment shape variation, Mast and Nelson [4] proposed a segmentation scheme for TMT that reduces the segment elongation. The basic approach is as follows:

1. Define an array of regular, equally-sized hexagons in the XY_{M1} plane. The hexagons are not separated by gaps at this point.
2. Apply a radial scaling rule to the location of the hexagon corners in the XY_{M1} plane. For simplicity, azimuth-dependant scaling rules were not considered.
3. Project the scaled hexagon corner locations along Z_{M1} onto the optical surface.
4. Adjust the locations of hexagon corners in the optical surface to obtain uniform inter-segment gaps.

The radial scaling rule applied in Step 2 (detailed in Section 2.3 below) acts to distort the pattern of hexagons in the XY_{M1} plane such that when they are projected onto the optical surface, the resultant hexagons are more nearly regular. This is shown schematically in Figure 8.

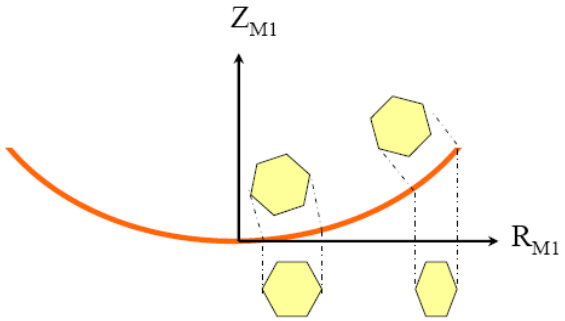

Fig. 8. Radius-dependent distortion of a planar hexagonal pattern. When the distorted hexagons are projected onto the optical surface, the resulting hexagonal outlines are more nearly regular.

In order to implement this approach, several metrics (i.e. quantities to be optimized by the segmentation approach) were identified. Two scaling rules were identified, and performance relative to the various metrics was evaluated.

2.2 Optimization metrics

Eight different optimization goals were considered during the process of determining the preferred segmentation approach for TMT. Each goal and its associated metric is defined and described in this section.

2.2.1 Minimize segment irregularity

"Irregularity" is a measure of the shape difference between an irregular hexagon (i.e. one where not all sides and/or angles are equal) and a regular hexagon. Mast and Nelson [4] constructed six center-to-corner lines in each hexagon, and

defined irregularity in terms of the variations in the lengths of and angles between those lines. A different approach was used in the implementation described in this paper.

In this paper, the measure of irregularity is defined as follows. Considering a planar, irregular hexagon, as shown in Figure 9, one can define a best fit regular hexagon (BFRH) as the planar regular hexagon that minimizes the sum of the squares of the distances d_i between each vertex of the irregular hexagon and the corresponding vertex of the BFRH, i.e.

$$\underset{c_x, c_y, \phi, a}{Min} \sum_{i=1}^{6} d_i^2 \tag{2}$$

where (c_x, c_y), φ, and a are the center location of the BFRH, its clocking angle, and its side length respectively. The irregularity of a given hexagon may then be expressed as the Root Mean Square (RMS) of the values of d_i (i.e. the residual of the best fit process) as follows:

$$\text{RMS Irregularity} = \sqrt{\frac{\sum_{i=1}^{6} d_i^2}{6}} \tag{3}$$

For optimizations relative to this parameter, the RMS Irregularity of the most irregular segment (of the 82 segment types) was minimized. This can be expressed as follows:

$$\underset{\text{scaling parameter}}{Min} \left(\underset{i=1 \cdots 82}{Max} \left(\text{RMS Irregularity}_i \right) \right) \tag{4}$$

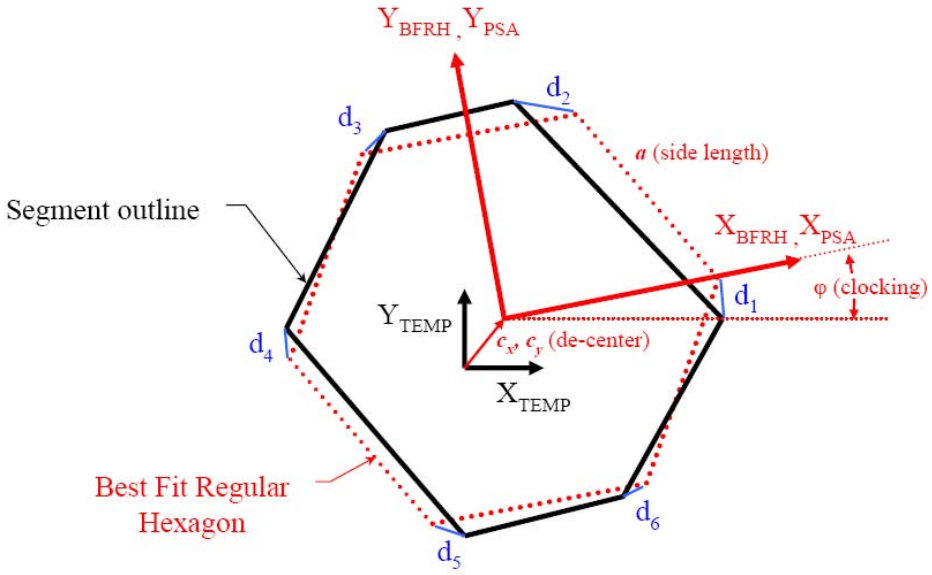

Fig. 9. Schematic showing the Best Fit Regular Hexagon (BFRH) associated with a given irregular hexagon. The "TEMP" coordinate system is a temporary coordinate system defined such that X_{TEMP} is parallel to the XZ_{M1} Plane. The "BFRH" coordinate system is established by the location and orientation of the BFRH, and is used to define the "Primary Segment Assembly" (PSA) coordinate system, the ultimate local coordinate system for the segment.

2.2.2 Minimize variation in segment area

Variations in segment area correspond directly to variations in segment mass. So by minimizing the variations in segment area, one can hope to reduce the degree of Segment Support Assembly tuning required to compensate for mass variations. The optimal adjustment of a scaling parameter for this goal can be expressed as follows

$$\underset{\text{scaling parameter}}{Min}\left(\frac{\underset{i=1\ldots82}{Max}(\text{Area}_i)}{\underset{i=1\ldots82}{Min}(\text{Area}_i)}-1\right) \tag{5}$$

2.2.3 Minimize variation in circumscribed diameter

The segments are fabricated from circular meniscus glass or glass-ceramic blanks. In order to minimize the fabrication cost of the blanks, it is desirable that all blanks be identical, and that the hexagonal segments be cut from the blanks with a minimum of waste. This can be accomplished by tuning the segmentation approach to minimize the variation in size of the circumscribed diameter of the hexagons. The optimal adjustment of a scaling parameter for this goal can be expressed as follows:

$$\underset{scaling\cdot parameter}{Min}\left(\frac{\underset{i=1\ldots82}{Max}(\text{Diameter}_i)}{\underset{i=1\ldots82}{Min}(\text{Diameter}_i)}-1\right) \tag{6}$$

2.2.4 Minimize diameter of largest circumscribed circle

As a variant of the metric described in 2.2.3, one can optimize the segmentation scheme such that the size of the largest circumscribed circle for any of the segments is minimized. This enables the use of the smallest possible standardized mirror blank.

2.2.5 Minimize range of length of mirror cell members

As described above, the nodes of the Mirror Cell are aligned with segment vertices. The segmentation approach therefore affects the locations of the nodes and the lengths of the truss members. Each of the 82 segments (i, equation 7) is mounted to three truss members (k, equation 7). The segmentation approach can be tuned to minimize the variation in length of the truss members (within the entire array), as described by the following:

$$\underset{\text{scaling parameter}}{Min}\left(\frac{\underset{i=1\ldots82,k=1\ldots3}{Max}(\text{L}ength_{i,k})}{\underset{i=1\ldots82,k=1\ldots3}{Min}(\text{L}ength_{i,k})}-1\right) \tag{7}$$

2.2.6 Minimize in-plane adjustment range between the SSA and the mirror cell

As described above, each Segment Support Assembly attaches to the Mirror Cell at three locations. For the TMT SSA it was decided that the three attachment features be equally spaced on a circle of a given radius for all 82 types, relative to the PSA coordinate system (i.e. the local segment system), allowing the same SSA components to be used universally. The hard-points on the mirror cell, where the SSA attaches, are located on the truss member, 1/3 of the way between cell nodes, and potentially offset uniformly in the Z_{PSA} direction to facilitate packaging.

Due to segmentation, these mirror cell attachment points vary relative to the SSA attachment features. To the extent that an SSA attachment feature and the mirror cell attachment points are not coincident, adjustment range of the SSA must be allocated. It follows that for any segmentation pattern, there is a best fit radius for the SSA attachment features that minimizes the required in-plane adjustment range. Since it is desirable to minimize the required adjustment range (smaller and less costly parts), it is necessary to determine the best-fit radius for the SSA attachment features, and the resulting range of travel required for each segmentation pattern that is considered.

The axial location (Z_{PSA}) of the SSA attachment features is chosen as the mean Z_{PSA} coordinate of all of the mirror cell attachment points (averaged across all segments) in order to minimize the vertical adjustment range. For the TMT SSA design, it was found that the Z_{PSA} adjustment range is consistently small and not a controlling design parameter.

Therefore, this metric is defined as the maximum in-plane distance between the interface point on the Mirror Cell and the interface point on the SSA (at the best fit radius). The optimum tuning can be described by the following:

$$\underset{\text{scaling parameter}}{Min}\left(\underset{i=1\ldots82,k=1\ldots3}{Max}\left(Dist\{Mirror\_Cell\_Interface_{i,k}, SSA\_Interface_{i,k}\}\right)\right) \tag{8}$$

2.2.7 Minimize magnitude of whiffletree pivot shifts

As described above, the variations in segment shape will be compensated for by shifting the locations of the whiffletree pivots. This implementation requires custom-drilling the pivot locations in the whiffletree hubs. It is desirable to minimize the magnitude of the required shifts: shifts of a few mm can easily be accommodated; shifts on the orders of centimeters would challenge packaging. In the final design implementation, a finite element model will be built for each segment type to determine and verify the optimum location for the pivots. To date, the magnitudes of the pivot shifts have only been estimated. Using the sensitivity analysis results described in section 1.5, a formula was developed that estimates the magnitude of pivot shifts, in mm, as follows:

$$Pivot\_Shift\_Magnitude = 0.49\left|R - R_{nom}\right| + 0.636(RMS\_Irregularity) \tag{9}$$

Where R is the radius of the circle circumscribing the given segment, R_{nom} is the mean circumscribed radius among all 82 segment types, and RMS_Irregularity is the quantity described in 2.2.1. Optimization for this parameter entails adjusting the scaling parameter to minimize the largest pivot shift magnitude amongst any of the 82 segment types.

2.2.8 Minimize residual RMS after whiffletree pivot shifts

The pivot shifts described above do not perfectly correct the surface figure of a segment. There is a gravity-induced residual surface error (relative to the gravity-induced surface error of a nominal segment). Based on the results of the sensitivity analysis described in section 1.5, a formula was developed that estimates the residual surface error. This residual surface error adds in quadrature to the error of a nominal segment.

$$\varepsilon_{surfRMS} = \sqrt{\left(0.425\left(R - R_{nom}\right)\right)^2 + \left(0.197 * RMS\_Irregularity\right)^2} \tag{10}$$

2.3 Scaling rules

2.3.1 α-rule scaling

Having introduced the parameters to be optimized by segmentation, we now turn to the implementation of the scheme. First, an array of regular, un-gapped hexagons is defined in the XY_{M1} plane. Since the primary mirror has six-fold symmetry, all calculations are done on one 60° sector, as shown in Figure 10. For the purposes of this paper, we assume that the inner diameter, outer diameter, number and configuration of hexagons are defined a priori. A scaling approach is needed to scale the "Base Pattern" in the XY_{M1} plane such that when the hexagons are projected along Z_{M1} as shown in Fig 7, the resulting hexagons optimally satisfy the various evaluation metrics. Mast and Nelson [4] developed the following scaling rule:

$$R_i = R_{0,i}\frac{1+\alpha\left(\frac{R_{\max}}{k}\right)^2}{1+\alpha\left(\frac{R_{0,i}}{k}\right)^2} \tag{11}$$

where $R_{0,i}$ and R_i are the radial coordinates of the segment corners or centers, expressed in the M1 coordinate system, before and after scaling, respectively. $R_{\max}$ is the radius of the outermost segment corner in the Primary Mirror, k is the paraxial radius of curvature of M1, and α is a scaling parameter which is adjusted experimentally to optimize the segmentation. The $1/(1+\alpha(R_{oi}/k)^2)$ term foreshortens the outer segments with respect to the inner segments in the base pattern. The $(1+\alpha(R_{\max}/k)^2)$ term adjusts the scaling such that changing the scaling parameter does not change the overall diameter of the Primary Mirror. Mast and Nelson used this scaling formulation to minimize segment irregularity (parameter 2.2.1 above). They numerically identified an optimal value for α of 0.242, based on their measure of irregularity.

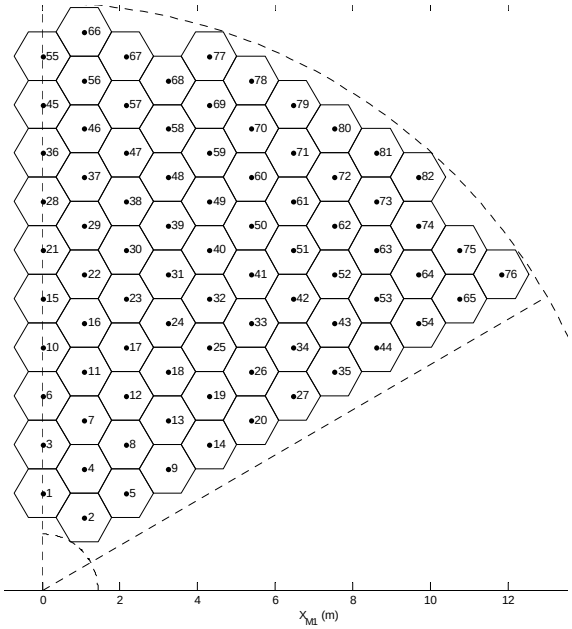

Fig. 10. The "Base Pattern" This is a pattern of regular, un-gapped hexagons in the XY_{M1} Plane. Due to the six-fold symmetry of the primary mirror, each of the 82 segment types are defined in Sector A. Coordinate transformations (rotating around Z_{M1} in 60° increments) are used to determine the segment parameters in the other sectors.

2.3.2 β-rule scaling

An alternate formulation was developed to investigate segment area variation and circumscribed circle diameter variation (parameters 2.2.2 and 2.2.3 above).

$$R_i = R_{0,i}\left[\frac{k}{R_{0,i}}\sin\left(\frac{R_{0,i}}{R_{\max}}\sin^{-1}\left(\frac{R_{\max}}{k}\right)\right)\right]^{\beta} \tag{12}$$

Parameters definition is the same as in equation 11, and "β" is a scaling parameter which is adjusted experimentally to optimize the segmentation. Though the form of this scaling rule is different than the α-rule, the function is similar. The $[(k/R_{oi})\sin(\{R_{01}/R_{max}\}\sin\text{-}1\{R_{max}/k\})]$ term generates a radius dependent multiplier that converges to 1 at $R_i=R_{max}$. The scaling parameter β scales the magnitude of the multiplier. By iterative computation, it has been determined that the value of β that minimizes segment area variation (parameters 2.2.2 above) is 0.708. The value of β that minimizes segment circumscribed circle diameter variation (parameters 2.2.3above) is 0.915.

2.3.3 Selection of scaling rule

The scale factors associated with the single-parameter-optimized cases described above are shown in Figure 11 below. The overall shapes of the curves produced by the two rules are very similar. The scaling parameters, α and/or β can be adjusted such that the scale factors generated by each rule are nearly identical. This is illustrated in Figure 11: an α-rule scaling with α=0.121 very closely approximates a β-rule scaling with β=0.708. When α and β are chosen such that the differences between the two scaling rules are minimized, the largest difference between the segment corner locations generated by the two rules is approximately 100μm. As such, it was concluded that the two scaling rules are functionally equivalent. Due to its simple expression, the α-rule was used for the detailed implementation of the segmentation calculations.

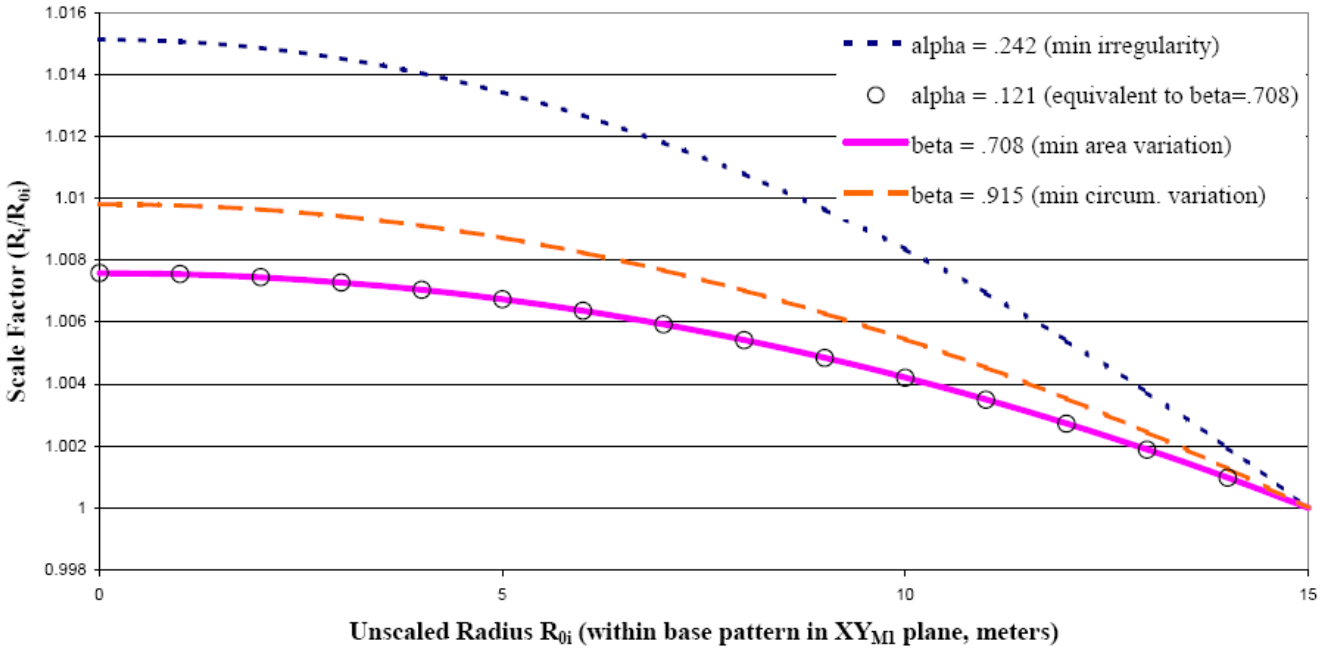

Fig. 11. Scale factors associated with a few values of the scaling parameters, α and β. The values of α and/or β may be chosen such that α-rule and β-rule scaling produce nearly identical results.

2.4 Computational implementation

A Matlab code was developed to automate the segmentation calculations and optimization. This code allows the user to input the scaling parameter α. The primary mirror paraxial radius of curvature and conic constant, the outer-diameter of the mirror array, and some basic dimensions of the SSA are defined within the code. Also specified are the parameters of the base pattern. The code outputs the location of all segment corners, the orientations of the local coordinate systems for each segment, the locations of each segment's interface points to the mirror cell, and detailed statistics for each of the optimization parameters listed in section 2.2. In order to accomplish this, the code steps through the following procedure:

1. Construct a planar array of regular hexagons with side length a=0.716m, in the XY_{M1} plane. Hexagons are clocked such that two corners are aligned along a line parallel to X_{M1}. One hexagon is centered at X_{M1}=Y_{M1}=0. Within each hexagon, corners are numbered counter-clockwise from 1 to 6. Corner #1 has the largest X_{M1} coordinate.
2. Create the inner and outer diameter of the array by removing hexagons whose center lies at a radius of less than 1.5m or greater than 14.4m
3. Identify six sectors of 82 hexagons each and number them A through F, counter-clockwise from sector A as seen from the stars. Sector A contains all segments centered on the $+Y_{M1}$ axis and has the rest of its segments entirely in the [$+X_{M1}$, $+Y_{M1}$] quadrant. Sector A is chosen as the master sector. Calculations need only be performed once, in the master sector. All other sectors (B through F) are identical copies of sector A, created by rotating about Z_{M1}, counter-clockwise as seen from the stars, by 60 degrees from each sector to the next. All subsequent calculations are performed on the Sector A base pattern, shown above in Figure 10.
4. Using the user-defined value of α, apply the radial scaling rule to the centers and vertices of the base pattern to produce the *scaled base pattern*.
5. Calculate the Z_{M1} coordinates of segment vertices (without gaps) and centers in the M1 optical surface, by projecting from the base pattern, parallel to Z_{M1}.

6. Calculate coordinates of Mirror Cell nodes (in XYZ_{MI}). At each of 3 corners (#1, 3, and 5) of each segment, define a mirror cell node at a given distance behind the optical surface, along the local normal to the optical surface at that vertex (without gaps).

7. Calculate the nominal coordinates of mirror cell's interface points. As described in section 1.3, these points are located at the 1/3 points of cell members, potentially offset uniformly in the Z_{PSA} direction to facilitate packaging

8. Define the XYZ_{TEMP} reference frame for each segment as follows: the origin is at the projected location of the temporary center defined in step 5. The Z_{TEMP} axis is normal to the local optical surface at the origin. The X_{TEMP} axis is parallel to the XZ_{MI} plane. As seen in projection in the XY_{MI} plane, the X_{TEMP} axis points in the same direction as the X_{MI} axis. The Y_{TEMP} axis completes a right-handed system.

9. Project the corners of each segment from the optical surface into the XY_{TEMP} plane associated with that segment (parallel projection along Z_{TEMP}). Connecting these points with straight line segments in the XY_{TEMP} plane forms the *zero-gap segment outline*.

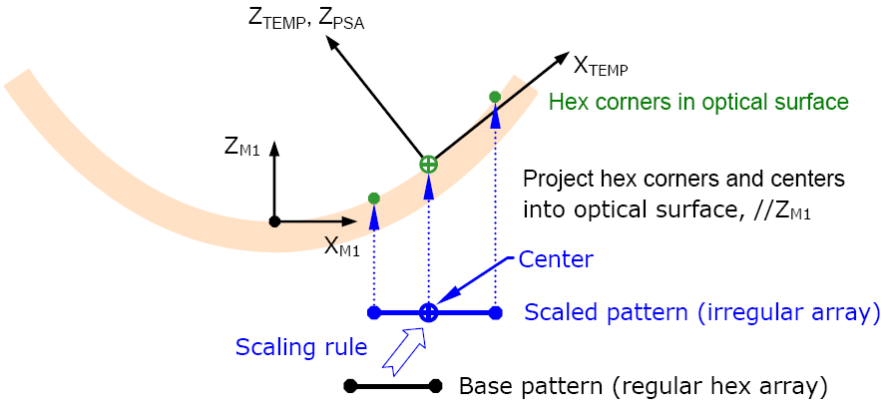

Fig. 12. Vertex projection and definition of temporary coordinate system.

10. For each segment, a half-gap is subtracted all around the edges of the zero-gap segment outline, producing the *segment outline* (straight-sided in the XY_{TEMP} plane).

11. Define a *best-fit regular hexagon* (BFRH) in the XY_{TEMP} plane that best approximates the irregular segment outline, as described in Section 2.2.1. Relative to the *TEMP* coordinate system of an irregular segment, a BFRH may be fully defined by its side length (size), clocking angle, and center location. In preliminary investigations, it was determined that whereas side length and clocking angle strongly affect the quality of the "fit" (i.e. the magnitude of the residual irregularity), allowing optimization of the BFRH center location does not. That is, the RMS irregularity of an irregular segment relative to a BFRH fit with size, clocking, and centration is not much better than the RMS irregularity of the same segment relative to a BFRH fit with size and clocking only. Due to the conceptual and computational complications that arise when the BFRH is allowed to de-center, it was decided to implement the fit using only size and clocking. Therefore, the segment and the BFRH share the same center, the position of which in X_{M1} and Y_{M1} is established by the scaling operation described in step 4.

12. Define the Primary Segment Assembly (*PSA)* coordinate system, based on the BFRH, as follows: the origin 0_{PSA} is coincident the center of the BFRH, Z_{PSA} is parallel to Z_{TEMP}. X_{PSA} points from 0_{PSA} to the #1 vertex of the BFRH (i.e. it is clocked relative to XYZ_{TEMP} by the best fit clocking angle). The Y_{PSA} axis completes a right-handed system. This system is then used to define the orientation of the Segment Support Assembly

13. Based on the Segment Support Assembly orientation defined in step 12 and the mirror cell attachment point coordinates, defined in step 7, the best-fit radius and axial location (height) for the SSA attachment points is calculated, followed by the calculation of the maximum adjustment travel range required to mate these two sets of features.

14. Calculate and output the value of all optimization metrics.

15. Calculate segment origins, corner locations, and PSA coordinate systems for sectors B through F, by transforming sector A results around the Z_{M1} axis in 60° increments.

3. RESULTS

The segmentation code was run using a range of values for the scaling parameter α. For each value of α, the values of the eight optimization metrics were recorded. The results are plotted below in Figure 13.

Of all of the optimization metrics, the size of the largest circumscribed circle (Section 2.2.4) has the clearest cost implications. By minimizing the size of the largest circumscribed circle, one can minimize the size of mirror blank required, thereby minimizing waste and reducing material costs. The value of the scaling parameter that optimizes the size of the largest circumscribed circle is α=0.165. As can be seen in Figure 13, this value of the scaling parameter is also favorable for a number of the other metrics. As such, it was adopted as the baseline value of the scaling parameter. The specific values of all of the optimization metrics, evaluated at α=0.165 are given in Table 1.

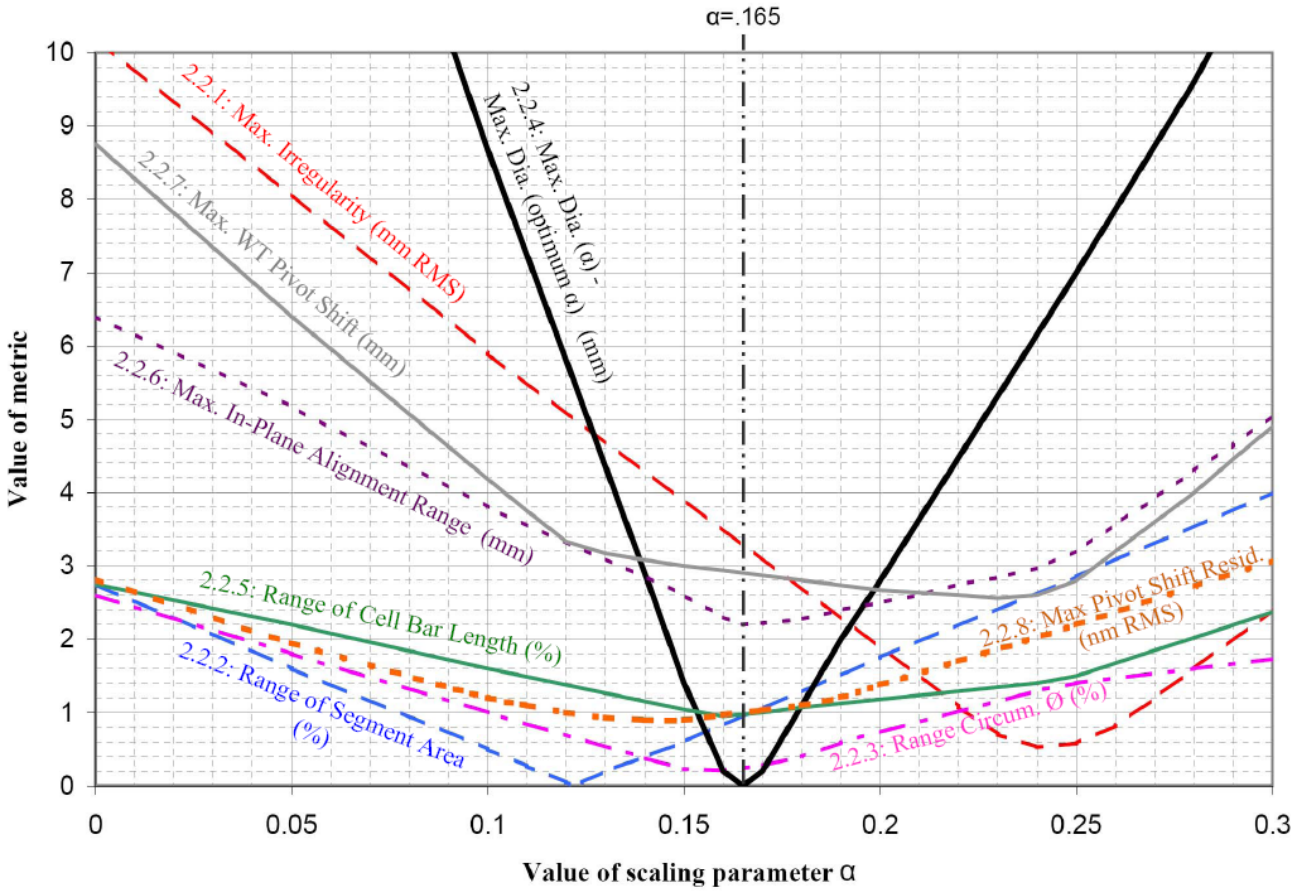

Fig. 13. Values of the eight optimization metrics evaluated at various values of the scaling parameter.

Table 1. Values of each of the optimization metrics, evaluated at the baseline value of the scaling parameter, α=.165

Parameter #	Optimization Goal	Result for α=.165
2.2.1	Minimize Segment Irregularity	Max = 3.245mm, at segment #66
2.2.2	Minimize Variation in Segment Area	Min = 1.3409m^2, at segment #82 Max = 1.3538m^2, at segment #2
2.2.3	Minimize Variation in Circumscribed Diameter	Min = 1.44057m, at segment #55 Max = 1.44406m, at segment #32
2.2.4	Minimize Diameter of Largest Circumscribed Circle	Max = 1.44406m, at segment #32
2.2.5	Minimize Range of Mirror Cell Member Length	Min = 1.2485m, Max = 1.2605m Range =12.0 mm
2.2.6	Minimize Adjustment between the SSA and the Mirror Cell	Max (in XY_{PSA}) = 2.19 mm Max (in Z_{PSA}) = .16mm
2.2.7	Minimize Magnitude of Whiffletree Pivot Shifts	Max = 2.84mm, at segment #66
2.2.8	Minimize Residual Surface RMS after Pivot Shifts	Max = 0.93nm RMS, at segment #66

4. SUMMARY

The TMT primary mirror consists of 492 hexagonal mirror segments separated by 2.5mm gaps. Because of the non-flat shape of the primary mirror and the desire to maintain uniform inter-segment gaps, the hexagonal outlines of the segments are neither identical nor regular. Size and shape variations among the segments have undesirable consequences, motivating the quantification and minimization of those variations. Eight metrics of segment size and shape variation were introduced, and a tunable method was described to define the irregular hexagon shapes of the segments. The computational implementation of the segmentation scheme was described. The optimum tuning was presented, and the values of the optimization parameters (geometric properties of the resulting segment geometry) obtained at the optimum tuning were tabulated.

5. ACKNOWLEDGEMENTS

The authors gratefully acknowledge the support of the TMT partner institutions. They are the Association of Canadian Universities for Research in Astronomy (ACURA), the California Institute of Technology and the University of California. This work was supported as well by the Gordon and Betty Moore Foundation, the Canada Foundation for Innovation, the Ontario Ministry of Research and Innovation, the National Research Council of Canada, the Natural Sciences and Engineering Research Council of Canada, the British Columbia Knowledge Development Fund, the Association of Universities for Research in Astronomy (AURA) and the U.S. National Science Foundation. The research carried out at the Jet Propulsion Laboratory, California Institute of Technology, was performed under a contract with the National Aeronautics and Space Administration.

REFERENCES

[1] Thirty Meter Telescope (TMT), http://www.tmt.org

[2] Ponslet, E.; Blanco, D.; Cho, M.; Mast; T.; Nelson, J.; Ponchione, R.; Sirota, M.; Stephens, V.; Stepp, L.; Tubb, A.; Williams, E. C., "Development of the Primary Mirror Segment Support Assemblies for the Thirty Meter Telescope", Atad-Ettedgui, E.; Antebi, J.; Lemke, D., Editors, SPIE Proceedings, Vol. 6273, 2006

[3] Williams, E. C.; Baffes, C.; Mast, T.; Nelson, J.; Platt, B.; Ponchione, R.; Ponslet, E.; Setoodeh, S.; Sirota, M.; Stephens, V.; Stepp, L.; Tubb, A., "Advancement of the Segment Support System for the Thirty Meter Telescope Primary Mirror", SPIE Proceedings, Marseille, 2008

[4] Mast, T. and Nelson, J, TMT-internal communication: TMT Primary Mirror Segment Shape, TMT Report No. 58 2004